Theoretical total cross sections for e-SO_2 scattering over a wide energy range (0.1−2000 eV) revealing a 3.4-eV shape resonance

Minaxi Vinodkumar,[1,*] Chetan Limbachiya,[2] Avani Barot,[1] and Nigel Mason[3]
[1]*V. P. & R. P. T. P Science College, Vallabh Vidyanagar–388 120, Gujarat, India*
[2]*P. S. Science College, Kadi–382 715, Gujarat, India*
[3]*Department of Physics and Astronomy, Open University, Milton Keynes, MK7 6AA, United Kingdom*
(Received 30 April 2012; published 18 July 2012)

We have used the *ab initio* R-matrix formalism at low impact energies (below the ionization threshold of the target) and the spherical complex optical potential methodology above the ionization threshold to generate total cross sections for e-SO_2 scattering over the energy range from 0.1 to 2000 eV. The eigenphase diagram and total cross section indicate a structure at 3.4 eV which is ascribed to a shape resonance, evidence for which appears in earlier experimental studies.

DOI: 10.1103/PhysRevA.86.012706 PACS number(s): 34.80.Bm

I. INTRODUCTION

Sulfur dioxide (SO_2) plays a key role in the formation of acid rain in the terrestrial atmosphere and, through the sulfate aerosols that it may form, produces cooling effects which can offset warming effects produced by CO_2 [1]. SO_2 has also been observed in the atmosphere of Venus and in the atmosphere of Jupiter and its satellite Io [2]. SO_2 has also been detected in the interstellar medium [3]. Owing to the structural similarities between SO_2 and ozone, SO_2 can also serve as a test molecule for understanding the dynamics of ozone production and decomposition in the earth's atmosphere since experiments on O_3 are difficult [4] to perform due to the reactivity of ozone with atmosphere.

Electron interactions with SO_2 play an important role in magnetospheric plasma dynamics of the Jovian system, in the plasma-assisted treatment of biocompatible materials and biomedical surfaces, in models of diffuse discharge switches [5], and in understanding the underlying physics and chemistry of combustion process. Low-energy collision processes are perhaps the most important phenomena since they underpin the physicochemical processes prevalent in the plasmas and many industrial discharges. At low energies (<10 eV) electrons may also cause short-lived anions (and thereby resonances) whose decay (to produce neutral and anionic fragments) may strongly influence the local chemistry.

Theoretical studies of low-energy electron scattering from SO_2 are nevertheless sparse and a critical review of such data reveals systematic discrepancies in the magnitude of the total cross section. Reviewing the literature on e-SO_2 scattering we can conveniently divide it into two regions of impact energies, one below and one above the ionization threshold (12.34 eV) of the target.

Concentrating first on a review of previous work conducted in the low-energy regime, several experimental measurements have been reported [6–10]. Gulley and Buckman [6] measured absolute differential cross sections for vibrationally elastic electron scattering using a crossed electron-molecular beam apparatus for incident energies of 1–30 eV. Zubek *et al*. [7], Szmytkowski and Maciag [8], and Szmytkowski *et al*. [9] have employed linear transmission experiments to measure total cross sections for incident energies 1.5–7 eV, 1.5–70 eV, and 6–370 eV, respectively, while Sokolov and Sokolova [10] measured total cross sections employing the electron cyclotron resonance technique in the energy range 1.5–10 eV. Sanche and Schulz [11] performed an electron transmission experiment to detect resonance structure in SO_2, identifying a broad shape resonance at 3.4 eV. This was subsequently confirmed by the measurements of Simon *et al*. [12] and Andric *et al*. [13], which showed the formation of a temporary SO_2^- state which decays to leave the molecule excited in one of its vibrational modes.

There are only a few calculations of low-energy e-SO_2 scattering. Gupta and Baluja [14] have calculated total elastic cross sections using the R-matrix method for impact energies 0–15 eV. Gianturco *et al*. [15] performed *ab initio* calculations for the energy range 0–30 eV and Natalense *et al*. [16] employed the Schwinger multichannel method and computed rotationally summed inelastic, differential and integral, and momentum transfer cross sections for electron scattering for impact energies from 3 to 30 eV. Very recently Machado *et al*. [17] reported the results of a joint theoretical (1–1000 eV) and experimental (100–1000 eV) study to determine total cross sections for e-SO_2 scattering. It should be noted that these earlier theoretical works [14–17] were not able to predict the shape resonance reported in Refs. [12,13].

Reviewing the available high-energy work there are two experimental measurements reported in the literature. Zecca *et al*. [18] measured total cross sections for e-SO_2 using the Ramsauer technique over the energy range 90–4000 eV. Machado *et al*. [17] used the relative flow technique and measured total cross sections over the range of 100–1000 eV. High-energy theoretical formalisms of the total cross sections were reported by Shi *et al*. [19] using the Spherical Complex Optical Potential (SCOP) formalism over the energy range 30–4000 eV, and Raj and Tomar [20] used the additivity rule to derive cross sections for impact energies between 100 and 4000 eV.

Thus reviewing previous work on e-SO_2 scattering it is notable that there are more experimental data [6–11,13,17] than theoretical investigations [11,12,14,15,17]. The other notable fact is that although e-SO_2 has been studied over

*minaxivinod@yahoo.co.in

TABLE I. Target properties of SO_2.

Properties of SO_2	Present	Theoretical results	Expt. results
Ground-state energy (Hartree)	–547.20	–547.28 (Ref. [14]); − 547.28 (Ref. [17]) − 567.23 (Ref. [15])	–
First excitation energy (eV)	3.794	3.75 (Ref. [14])	3.40 (Ref. [29]); 3.5 (Ref. [30])
Rotational constant (cm^{-1})	2.025	3.0 (Ref. [15])	2.025 (Ref. [22])
Dipole moment (D)	2.1	2.4 (Ref. [14]) 1.92 (Ref. [16])	1.63 (Refs. [6,12,29])

a wide range of impact energies, all of the previous groups have carried out work over a limited range of impact energies. The present work is therefore unique as we have investigated the total cross section over a wide energy range starting from 0.1 eV to a high energy of 2000 eV, and we are able to detect the resonance at 3.4 eV as predicted by Sanche and Schulz [11] and confirmed by Simon *et al*. and Andric *et al*. [12,13]. Similarly we are able to theoretically confirm the shape resonance at 5.1 eV as detected by Gulley and Buckman [6].

The present work is carried out using two distinct formalisms since a single formalism cannot be employed over the extensive energy range as presented here. At low impact energies (below the ionization threshold of the target) we have carried out *ab initio* calculations using the *R*-matrix formalism through the Quantemol-N package [21–24], and above the threshold of the target, the SCOP formalism [25] is employed. Both the formalisms are well established and consistent over their respective range of impact energies. We therefore employed the *R*-matrix code to carry out *ab initio* calculations to find total (elastic plus electronic excitation) cross sections up to the ionization threshold of the target and the spherical complex optical potential (SCOP) method for calculating total (elastic plus inelastic) cross sections beyond the ionization threshold up to 2 keV [26]. The composite results obtained by combining them has been shown to be promising [21,22,26] as there is consistency in the data particularly at the transition energy (∼15 eV) where the two formalisms overlap. Hence the main incentive for the present work is threefold: (i) to detect the resonance structures at low energies, (ii) to provide total cross sections over an extensive range of impact energies, and (iii) to benchmark our results against previous experimental and theoretical data. In the next section we will briefly outline the two theoretical formalisms employed.

II. THEORETICAL METHODOLOGY

Before discussing theoretical methodology in detail we outline the target model employed for low-energy calculations.

A. Target model

SO_2 is a bent molecule with a bond length of 2.707 a.u. and an O-S-O angle of 119.3° [27]. We employed a double zeta plus polarization (DZP) Gaussian basis set for target wave function representation. SO_2 has C_{2v} symmetry of order 4. The ground-state electronic configuration is represented as $^1A_1^2$, $^1B_2^2$, $^2A_1^2$, $^3A_1^2$, $^2B_2^2$, $^1B_1^2$, $^4A_1^2$, $^5A_1^2$, $^3B_2^2$, $6A_1^2$, $^4B_2^2$, $^7A_1^2$, $^2B_1^2$, $^5B_2^2$, $^1A_2^2$, $^8A_1^2$. Out of 32 electrons we have frozen 14 electrons in the $^1A_1$, $^2A_1$, $^3A_1$, $^4A_1$, $^1B_1$, $^1B_2$, $^2B_2$ molecular orbitals while the remaining 18 electrons are kept free in the active space of $^5A_1$, $^6A_1$, $^7A_1$, $^8A_1$, $^2B_1$, $^3B_1$, $^3B_2$, $^4B_2$, $^5B_2$, $^1A_2$ molecular orbitals. A total of 1406 configuration state functions (CSFs) are used for accurate representation of the eight total target states. This large number of CSFs should ensure a correct determination of resonance peaks particularly in the low-energy regime. The number of channels included in the *R*-matrix calculations is 240.

The Quantemol-N modules GAUSPROP and DENPROP [28] construct the transition density matrix from the target eigenvectors obtained from configuration integration (CI) calculation and generate the target properties. The multipole transition moments obtained are then used to solve the outer region coupled equations and the dipole polarizability α_0. These are computed using second-order perturbation theory and the property integrals are evaluated by GAUSPROP. Our self-consistent field (SCF) model calculations yielded target parameters such as the ground-state energy, the first electronic excitation energy, the rotational constant, and the dipole moment which are all listed in Table I.

From the present CI calculations the ground-state energy for SO_2 is − 547.20 hartree which is in excellent agreement with − 547.28 hartree reported by Gupta and Baluja [14] and − 547.28 hartree reported by Machado *et al*. [17], but higher than the theoretical value of − 567.232 hartree reported by Gianturco *et al*. [15] by 20 hartree. The excitation energy of the first excited state is calculated to be 3.794 eV, which is in excellent agreement with the theoretical value of 3.75 eV predicted by Gupta and Baluja [14] and is close to the experimental value of 3.4 eV reported by Flicker *et al*. [29] and 3.5 eV reported by Vuskovic and Trajmar [30]. The rotational constant obtained in the present calculation is 2.025 cm^{-1} and is in excellent agreement with the experimental value of 2.02 cm^{-1} from Computational Chemistry Comparison and Benchmark Database (CCCBDB) [27] but, again, lower than the theoretical value of 3.0 cm^{-1} reported by Gianturco *et al*. [15]. The present dipole moment at the equilibrium geometry is 2.1 D, which is comparable with the experimental value of 1.63 D [6] and slightly higher than the theoretical value of 1.92 D predicted by Natalense *et al*. [16] and lower than the 2.4 D reported by Gupta and Baluja [14]. The calculated 14 vertical electronic excitation thresholds for SO_2 are reported in Table II.

B. Low-energy formalism (0.1 to ∼15 eV)

The most popular methodologies employed for low-energy electron collision calculations are the Kohn variational method, the Schwinger variational method, and the *R*-matrix method, of which the *R* matrix is perhaps the most widely

TABLE II. Vertical excitation energy of e-SO_2 up to ionization threshold.

State	Energy (eV)	State	Energy (eV)	State	Energy (eV)	State	Energy (eV)
$^1A_1$	0.000	$^3A_2$	5.156	$^1A_2$	8.856	$^1A_1$	10.103
$^3B_1$	3.798	$^1A_2$	5.314	$^1B_1$	9.164	$^3B_2$	10.761
$^3B_2$	4.851	$^1B_2$	8.097	$^1A_1$	9.311	$^3A_2$	11.762
$^1B_1$	4.876	$^3A_1$	8.633	$^3B_2$	9.575		

used method [31]. The *ab initio* R-matrix method relies on the division of configuration space into two spatial regions, viz., an inner region and an outer region. This spatial distribution is a consequence of electronic charge distribution around the center of mass of the system. The inner region is chosen such that it accommodates the total wave function of the target molecule. Thus all the $N + 1$ electrons are contained in the inner region which makes the problem numerically complex, but very precise. The interaction potential consists of short-range exchange and electron-electron correlation polarization potentials. Moreover the inner region problem is solved independently of the energy of the scattering electron. In the outer region exchange and correlation are assumed to be negligible and the only long-range multipolar interactions between the scattering electron and the target are included. A single-center approximation is assumed here since this enables simple and fast solutions in the outer region. For the present system the inner R-matrix radius is taken as $10a_o$ while the outer region calculations are extended up to $100a_o$.

The inner region wave function is constructed using the close-coupling approximation [32]. In the inner region the total wave function for the system is written as

$$\psi_k^{N+1} = A \sum_I \psi_I^N(x_1, \ldots, x_N) \sum_j \zeta_j(x_{N+1}) a_{Ijk} + \sum_m \chi_m(x_1, \ldots, x_{N+1}) b_{mk}, \quad (1)$$

where A is the antisymmetrization operator, x_N is the spatial and spin coordinate of the nth electron, ξ_j is a continuum orbital spin-coupled with the scattering electron, and a_{Ijk} and b_{mk} are variational coefficients determined in the calculation. The accuracy of the calculation depends solely on the accurate construction of this wave function given in Eq. (1). The first summation runs over the target states used in the close-coupled expansion and a static exchange calculation has a single Hartree-Fock target state in the first sum. The summation in the second term runs over configurations χ_m, where all electrons are placed in target molecular orbitals. This sum runs over the minimal number of configurations, usually three or fewer, which are required to relax orthogonality constraints between the target molecular orbitals and the functions used to represent the configuration. Our fully close-coupled calculation uses the lowest number of target states, represented by a configuration interaction (CI) expansion in the first term and over 100 configurations in the second. These configurations allow for both orthogonality relaxation and short-range polarization effects.

The complete molecular orbital representation in terms of occupied and virtual target molecular orbitals are constructed using the Hartree-Fock self-consistent field method with Gaussian-type orbitals (GTOs) and the continuum orbitals of Faure *et al.* [33] and include up to g ($l = 4$) orbitals. The benefit of employing partial wave expansion for low-energy electron molecule interaction is its rapid convergence. In the case of dipole-forbidden excitations ($\Delta J \neq 1$) the convergence of the partial waves is rapid, but in the case of dipole-allowed excitations ($\Delta J = 1$) the partial wave expansion converges slowly due to the long-range nature of the dipole interaction. In order to account for the higher partial waves not included in the fixed-nuclei T matrices, the Born correction is applied. For low partial waves ($l \leqslant 4$) T matrices computed from the R-matrix calculations are employed to compute the cross sections. The low partial wave contribution arising from the Born contribution may be subtracted in order that the final rotational cross-section set only contains those partial waves due to R-matrix calculation. We have performed the calculations with and without a dipole Born correction.

The R matrix provides the link between the inner region and outer region. For this purpose the inner region is propagated to the outer region potential until its solutions match with the asymptotic functions given by the Gailitis expansion [34]. Thus by generating the wave functions, using Eq. (1), their eigenvalues are determined. These coupled single-center equations describing the scattering in the outer region are integrated to identify the K-matrix elements. Consequently the resonance positions, widths, and various cross sections can be evaluated using the T matrix obtained from the S matrix, which is in turn obtained from the K-matrix element.

C. High-energy formalism (15–2000 eV)

In the intermediate- and high-energy regime a conventional close-coupling theory [32] of an electron-molecule system is a complex and arduous task even with present day supercomputers. Hence many groups [17,19,24,25] employ spherical complex optical potential formalism in this region as it is consistent and simple and provides computationally fast solutions. The SCOP formalism [35,36] employs a partial wave analysis to solve the Schrödinger equation with various model potentials as its input. The interaction of incoming electrons with the target molecule can be represented by a local complex potential comprised of real and imaginary parts as

$$V_{\text{opt}}(E_i, r) = V_R(E_i, r) + i V_I(E_i, r), \quad (2)$$

such that

$$V_R(r, E_i) = V_{st}(r) + V_{\text{ex}}(r, E_i) + V_p(r, E_i), \quad (3)$$

where E_i is the incident energy. Equation (3) corresponds to various real potentials to account for the electron-target interaction, namely, static, exchange, and the polarization potentials, respectively. These potentials are obtained using the

molecular charge density of the target, the ionization potential, and the polarizability as inputs. We describe the scattering process within the confines of the fixed-nuclei approximation which neglects any dynamics involving the nuclear motion (rotational and vibrational), with the bound electrons being assumed to be in the ground electronic state of the target at its optimized equilibrium geometry. The molecular charge density may be derived from the atomic charge density by expanding it from the center of mass of the system. Thus, the single-center molecular charge density is obtained by a linear combination of constituent atomic charge densities, renormalized to account for covalent molecular bonding.

The atomic charge densities and static potentials ($V_{\rm st}$) are formulated from the parametrized Hartree-Fock wave functions given by Cox and Bonham [37]. The parameter-free Hara's "free electron gas exchange model" [38] is used to generate the exchange potential ($V_{\rm ex}$). The polarization potential (V_p) is constructed from the parameter-free model of correlation-polarization potential given by Zhang *et al.* [39]. Here, various multipole nonadiabatic corrections are incorporated in the intermediate region which will approach the correct asymptotic form at large "r" smoothly. In the low-energy region, the small r region is not important due to the fact that higher-order partial waves are unable to penetrate the scattering region. However, in the present energy region, a large number of partial waves contributes to the scattering parameters such that a correct short-range behavior of the potential is essential.

The imaginary part in $V_{\rm opt}$ is called the absorption potential $V_{\rm abs}$ and accounts for the total loss of flux scattered into the allowed electronic excitation or ionization channels. $V_{\rm abs}$ is not a long-range effect and its penetration towards the origin increases with increasing e energy. This implies that at high energies, the absorption potential accounts for the inner-shell excitations and ionization processes that may be neglected at low energies.

The well-known quasi-free-model form of Staszeweska *et al.* [40] is employed for the absorption part and is given by

$$V_{\rm abs}(r,E_i) = -\rho(r)\sqrt{\frac{T_{\rm loc}}{2}}\left(\frac{8\pi}{10k_F^3E_i}\right)\theta\left(p^2-k_F^2-2\Delta\right) \times (A_1+A_2+A_3), \quad (4)$$

where the local kinetic energy of the incident electron is

$$T_{\rm loc} = E_i - (V_{\rm st}+V_{\rm ex}+V_p), \quad (5)$$

and where $p^2 = 2E_i$, $k_F = [3\pi^2\rho(r)]^{1/3}$ is the Fermi wave vector and $\theta(x)$ is the Heaviside unit step function such that $\theta(x) = 1$ for $x \geqslant 0$, and is zero elsewhere. A_1, A_2, and A_3 are dynamic functions that depend differently on $\theta(x)$, I, Δ, and E_i. Here, Δ is the principal factor which decides the values of total inelastic cross section, since below this value ionization or excitation is not permissible. This is one of the main characteristics of the Staszewska model [40,41]. In the original Staszewska model [40,41] $\Delta = I$ is considered and hence ignores the contributions coming from discrete excitations at lower incident energies. This was recognized by Garcia and Manero [42] who discussed the need to modify Δ value. In the present calculation we consider Δ as a slowly varying function of E_i around I. Such an approximation is meaningful since Δ fixed at I would not allow excitation at energies $E_i \leqslant I$. Alternatively, if Δ is much less than the ionization threshold, then $V_{\rm abs}$ becomes unexpectedly high near the peak position. The amendment we introduced gives a reasonable minimum value $0.8I$ to Δ [43] and expresses the parameter as a function of E_i around I, i.e.,

$$\Delta(E_i) = 0.8I + \beta(E_i - 1). \quad (6)$$

Here the value of the parameter β is obtained by requiring that $\Delta = I$ (eV) at $E_i = E_p$, the value of incident energy at which $Q_{\rm inel}$ reaches its peak. E_p can be found by calculating $Q_{\rm inel}$ by keeping $\Delta = I$. Beyond E_p, Δ is kept constant and is equal to I. The theoretical basis for having a variable Δ is discussed in more detail by Vinodkumar *et al.* [43]. The expression (6) is meaningful since if Δ is fixed at the ionization potential it would not allow any inelastic channel to open below I, and if it is very much less than I, then $V_{\rm abs}$ become significantly high close to the peak position of $Q_{\rm inel}$.

The complex potential formulated in this way is used to solve the Schrödinger equation numerically through a partial wave analysis. This calculation will produce complex phase shifts for each partial wave which carries the signature of interaction of the incoming projectile with the target. At low impact energies only a few partial waves are significant, but as the incident energy increases more partial waves are needed for convergence. The phase shifts (δ_l) thus obtained are employed to find the relevant cross sections, total elastic (Q_{el}), and the total inelastic cross sections ($Q_{\rm inel}$) using the scattering matrix $S_l(k) = \exp(2i\delta_l)$ [44]. Total cross sections such as the total elastic (Q_{el}) and the total inelastic cross sections ($Q_{\rm inel}$) can then be derived from the scattering matrix [34]. The sum of these cross sections then gives the total scattering cross section (TCS) Q_T [35].

III. RESULTS AND DISCUSSION

We have carried out a comprehensive set of calculations on electron scattering from SO_2 between ~0.1 and 2000 eV. The results are represented graphically in Figs. 1–4 along with the available comparisons and numerical values which are tabulated in Table III.

Let us consider Figs. 1(a), 1(b), and 2, which show the total scattering cross-section curves. For clarity we have separated comparisons between the present results with experiments [Figs. 1(a) and 1(b)] and theory (Fig. 2). Below the ionization threshold calculations were performed using the R-matrix code and above it the SCOP formalism was employed. As evident from Figs. 1(b) and 2 the data produced by these two formalisms are consistent at the transition energy (~15 eV), and it validates the use of the two formalisms to provide a self-consistent TCS over such an extensive energy range. We have employed two models for our low-energy calculations, one employing the Born correction and other without the Born correction.

Figure 1(a) shows a comparison of present total cross sections with the experiments for low impact energies up to 10 eV. There are two important features to be observed in the low-energy regime; first, there is clear evidence for the presence of structure at 3.4 eV in the TCS curve

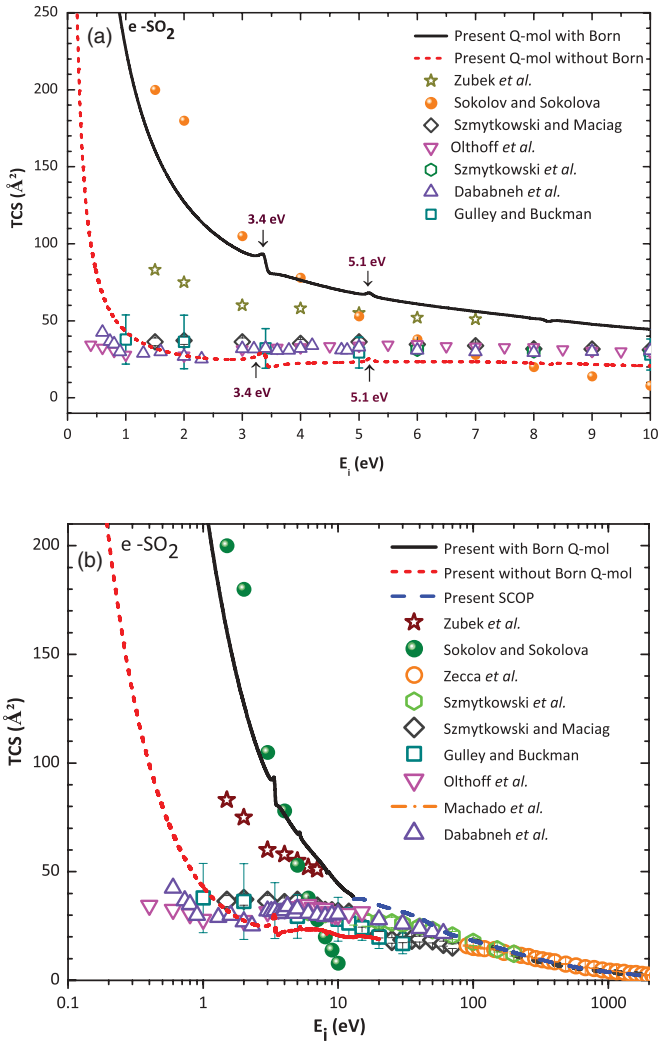

FIG. 1. (Color online) (a) Low-energy total cross section for e-SO_2 scattering compared with experiments. (Solid line) Present results (Q-mol with Born correction); (short dash line) present results (Q-mol without Born correction); (spheres) Sokolov and Sokolova [10]; (stars) Zubek *et al*. [7]; (open squares) Gulley and Buckman [6]; (open diamonds) Szmytkowski and Maciag [8]; (open hexagons) Szmytkowski *et al*. [9]; (open upward triangles) Dababneh *et al*. [45]; (open downward triangles) Olthoff *et al*. [46]. (b) Total cross section for e-SO_2 scattering compared with experiments. (Solid line) Present results (Q-mol with Born correction); (short dash line) present results (Q-mol without Born correction); (dash line) present results (SCOP); (stars) Zubek *et al*. [7]; (spheres) Sokolov and Sokolova [10]; (open circles) Zecca *et al*. [18]; (open hexagons) Szmytkowski *et al*. [9]; (open diamonds) Szmytkowski and Maciag [8]; (open squares) Gulley and Buckman [6]; (open upward triangles) Dababneh *et al*. [45]; (open spheres) Machado *et al*. [17]; (open downward triangles) Olthoff *et al*. [46].

which coincides with the observation of a resonance. Such a resonance was first observed by Sanche and Schulz [11] and subsequently confirmed by the measurements of Simon *et al*. [12] and Andric *et al*. [13] who showed the temporary formation of the SO_2^- state which decays into vibrational excitation of the neutral. Andric *et al*. [13] further confirmed that the symmetry of this state was most likely $^2B_2$ with the

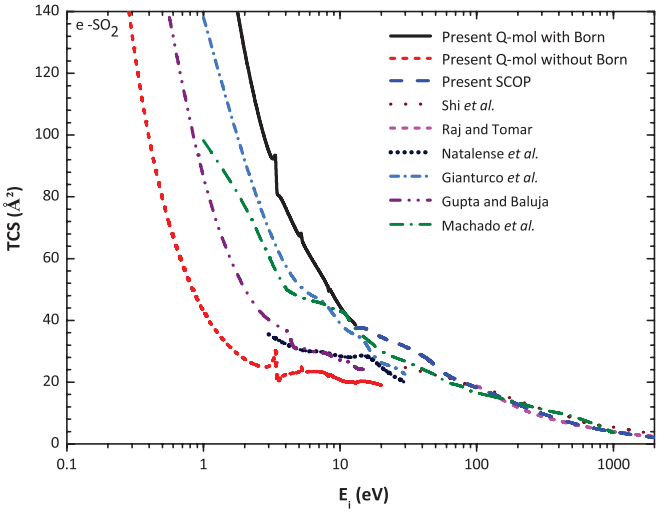

FIG. 2. (Color online) Total cross section for e-SO_2 scattering compared with theory. (Solid line) Present results (Q-mol with Born correction); (short dash line) present results (Q-mol without Born correction); (dash line) present results (SCOP); (short dash-dot line) Gianturco *et al*. [15]; (short dot line) Natalense *et al*. [16]; (dash-dot-dot line) Gupta and Baluja [14]; (dash-dot line), Machado *et al*. [17]; (dotted line) Shi *et al*. [19]; (bold short dashed line) Raj and Tomar [20].

additional electron being in the $^6B_2$ orbital. This resonance is reproduced exactly at 3.4 eV in our *ab initio* calculations using the R matrix shown by the arrow but it was not observed in the earlier calculations of Gupta and Baluja [14], Gianturco *et al*. [15], Natalense *et al*. [16], and Machado *et al*. [17]. The second feature observed in the present TCS is a weak structure at 5.1 eV which was also observed as a broad minimum by Gulley and Buckman [6] in their Differential Cross Section (DCS) measurement at 5 eV between 20° and 50°.

Figure 1(b) shows a comparison of electron-impact total cross sections for e-SO_2 scattering with experimental results from 0.1 to 2000 eV. Electron interactions with SO_2 have

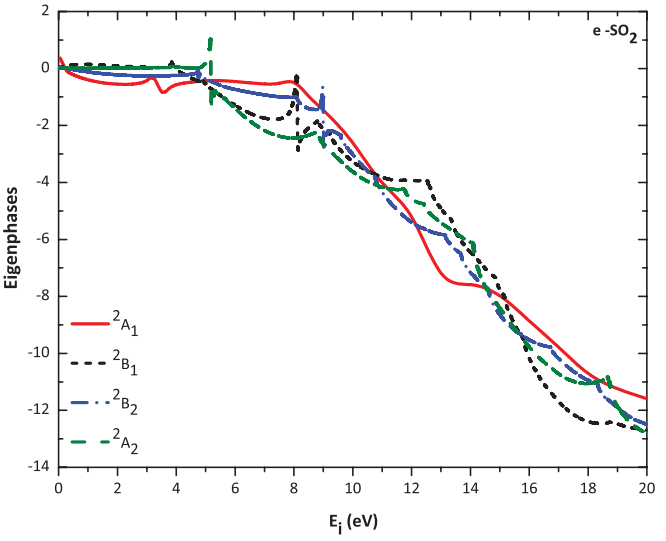

FIG. 3. (Color online) e-SO_2 eigenphase sums for an R-matrix eight-state Close Coupling (CC) calculation.

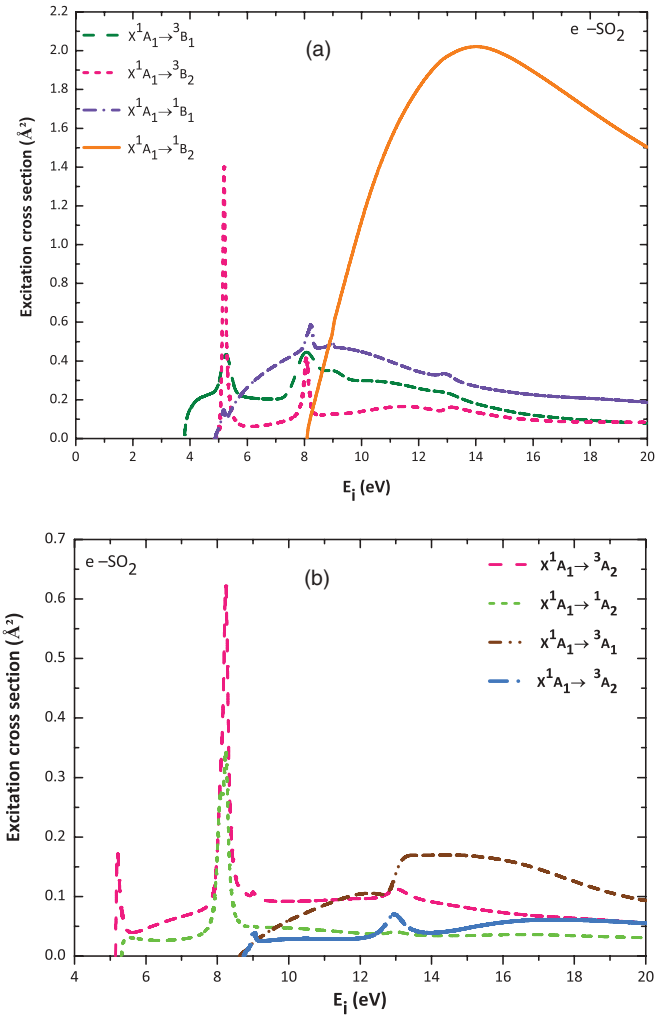

FIG. 4. (Color online) (a) e-SO_2 excitation cross sections for an eight-state CC calculation from initial state $^1A_1$: (Solid curve) $X\ ^1A_1 \rightarrow\ ^3B_1$ symmetry; (dashed curve) $X\ ^1A_1 \rightarrow\ ^3B_2$ symmetry; (dotted curve) $X\ ^1A_1 \rightarrow\ ^1B_1$; (dash-dot line) $X\ ^1A_1 \rightarrow\ ^1B_2$. (b) e-SO_2 excitation cross section for an eight-state CC calculation from initial state $1A_1$. (Dash curve) $X\ ^1A_1 \rightarrow ^3A_2$ symmetry; (short dash curve) $X\ ^1A_1 \rightarrow ^1A_2$ symmetry; (short dash-dot-dot curve) $X\ ^1A_1 \rightarrow ^3A_1$ symmetry; (dash-dot curve) $X\ ^1A_1 \rightarrow ^3A_2$ symmetry.

been extensively studied, interestingly with more experimental investigations [6–10,17,18] being reported than theoretical study [14–20]. The present results are in good agreement with most measured total cross sections if Born corrections are not included, suggesting that the Born corrected data overestimate the total cross section.

The overestimation in the Born corrected data is attributed to a larger value (30% higher compared to experimental value) of the dipole moment. Experimental values for integral cross sections are basically obtained by visual extrapolation of measured differential cross section over those angles which are not accessible experimentally. This introduces a large error in the low-energy regime below 2 eV [17]. The data of Szmytkowski *et al.* [9], Zubek *et al.* [7], and Sokolov and Sokolova [10] are considerably higher than all other data sets, perhaps an overestimation of the effects of forward scattering as discussed above and should therefore be considered as outliers.

TABLE III. Total cross sections of e-SO_2.

E_i (eV)	TCS (Å²) (with Born correction)	TCS (Å²) (without Born correction)	E_i (eV)	TCS (Å²) (SCOP)
0.1	1581.51	384.02	20	34.56
0.2	891.79	192.40	25	32.81
0.3	631.39	128.20	30	31.47
0.4	493.03	96.60	36	29.67
0.5	406.72	78.01	40	28.51
1.0	224.39	42.57	50	25.14
2.0	126.78	27.41	60	22.43
3.0	94.66	25.16	70	20.84
3.4	86.02	23.82	80	19.81
4.0	76.27	22.42	90	18.96
5.0	67.48	23.35	100	18.18
5.1	67.40	24.04	200	12.79
6.0	60.93	23.43	300	9.82
7.0	56.05	23.49	400	7.98
8.0	51.41	22.43	500	6.74
9.0	47.64	21.58	600	5.84
10	44.44	20.74	700	5.16
11	41.80	20.14	800	4.63
12	40.13	20.02	900	4.21
13	37.31	19.73	1000	3.86
14	37.65	20.24	1500	2.73
15	37.47	20.26	2000	2.11

Figure 2 depicts the comparison of present total cross sections for e-SO_2 scattering with other theoretical data over a wide range of impact energies from 0.1 to 2000 eV. Low-energy electron scattering calculations have been reported by four groups, Gupta and Baluja [14], Gianturco *et al.* [15], Natalense *et al.* [16], and Machado *et al.* [17]. SO_2 has a strong permanent dipole moment, 1.63 D, which is clearly reflected in the TCS curve as a steep fall in the elastic cross sections at low energies. The data of Gianturco *et al.* [15] and Natalense *et al.* [16] appear to overestimate the cross section while the two R-matrix-based results, present and that of Gupta and Baluja [14], appear to provide data that match the experimental results at least to energies as low as 2–3 eV. It is also clearly seen that inclusion of additional partial waves, through the Born correction, results in a much higher low-energy cross section which is greatly in excess of the majority of the experimental data and theoretical calculations. This overestimation in the Born corrected data is due to the strong dipole moment of 1.63 D of the SO_2 molecule. It is to be noted that above the ionization threshold the results obtained using SCOP formalism are in excellent agreement with all three [17,19,20] theoretical results, which reflects the consistency of SCOP formalism.

Having observed the clear evidence of resonant structures (at 3.4 and 5.1 eV) in the total cross-section curve it was necessary to study the eigenphase diagrams for the e-SO_2 system to confirm the presence of resonance structures. Figure 3 shows the eigenphase diagram for four doublet scattering states ($^2A_1$, $^2B_1$, $^2B_2$, $^2A_2$) of the e-SO_2 system. The $_2A^1$ state shows a prominent structure at 3.4, 8.17, and 13.05 eV. The prominent structure leads to the resonance peak

at 3.4 eV in the TCS curve as observed in earlier experiments [11–13]. The doublet A_2 state also shows a distinct structure at 5.1 eV which matches the broad minima observed by Gulley and Buckman [6] in their DCS measurement at 5 eV between 20° and 50°.

Figures 4(a) and 4(b) represent electron-impact excitation cross sections for ground state ${}_1A^1$ to the first eight excited states ${}^3B_1$, ${}^3B_2$, ${}^1B_1$, ${}^3A_2$, ${}^1A_2$, ${}^1B_2$, ${}^3A_1$, and ${}^3A_2$. For clarity we have shown the excitation cross-section curves for excited states for ${}^3B_1$, ${}^3B_2$, ${}^1B_1$, and ${}^1B_2$ in Fig. 4(a) and ${}_3A^2$, ${}_1A^2$, ${}_3A^1$, and ${}_3A^2$ in Fig. 4(b). Transitions to excited states ${}_3B^1$ and ${}_3B^2$ symmetry are in accordance with the dipole selection rule and show a strong peak in the cross section. The excitation cross section due to transition from ground state $X\,{}^1A_1$ to ${}^3B_2$ rises as a strong peak at 5.1 eV and corresponds to the shape resonance in ${}_2A^1$ symmetry due to its higher transition moment [14]. The excitation cross-section curve then flattens and shows a small peak at 8.1 eV. The same structure is also observed in the transition from $X\,{}_1A^1$ to ${}^3B_1$. The excitation cross section arising due to the transition from $X\,{}^1A_1$ to ${}^1B_1$ rises slowly, attains a broad peak around 8 eV, and then slowly decreases. Finally the excitation cross section arising due to the $X\,{}^1A_1$ to ${}^1B_2$ transition starts at 8 eV and reaches a broad maximum around 14 eV before gradually decreasing.

The excitation cross sections for the remaining four states of A-type symmetries are shown in Fig. 4(b). It is evident from the figure that transition from ground state $X\,{}^1A_1$ to ${}^3A_2$ is more prominent compared to ${}^1A_2$, and the excitation cross sections due to both transitions show strong peaks at 5.1 and 8.1 eV.

IV. CONCLUSION

In this paper we report results of theoretical calculations of electron scattering from sulfur dioxide over a wide energy range from 0.1 to 2000 eV. We have used the *ab initio* R-matrix formalism at low impact energies (below the ionization threshold of the target) and the spherical complex optical potential (SCOP) methodology above the ionization threshold; the two methods are shown to produce comparable cross sections at 15 eV. Both the eigenphase diagram and total cross section indicate a structure at 3.4 eV which is ascribed to a shape resonance which has been reported in earlier experimental studies. There is also detection of a second weaker resonance at 5.1 eV for which there is also some experimental evidence. We also report estimates of electronic state excitation cross sections.

The paper reviews all previous experimental and theoretical data and therefore provides a survey, that with the present consistent set of data, may be used to recommend a self-consistent set of total scattering cross sections from SO_2 that may be used in plasma and other applied studies. Indeed we would recommend the data in Table III be used as a preferred data set for the extensive energy range (0.1–2000 eV) with a 30% uncertainty, particularly at low energy below ionization threshold.

ACKNOWLEDGMENTS

M.V.K. acknowledges DST, New Delhi, for the major research project (SR/S2/LOP/26-2008), and C.G.L. thanks UGC, New Delhi, for the major research project [F. No.40-429/2011 (SR)] for financial support under which part of this work is carried out.

[1] A. Zeeca and R. S. Brusa, Nuovo Cimento **14C**, 481 (1991).
[2] A. Bhardwaj and M. Michael, Geophys. Res. Lett. **26**, 393 (1999).
[3] C. M. Persson, A. O. H. Olofsson, N. Koning, P. Bergman, P. Bernath, J. H. Black, U. Frisk, W. Geppert, T. I. Hasegawa, Å. Hjalmarson, S. Kwok, B. Larsson, A. Lecacheux, A. Nummelin, M. Olberg, Aa. Sandqvist, and E. S. Wirström, Astron. Astrophys. **476**, 807 (2009).
[4] J. A. Davies, W. M. Johnstone, N. J. Mason, P. Biggs, and R. P. Wayne, J. Phys. B **26**, L767 (1993).
[5] J. Marling, IEEE J. Quantum Electron. **14**, 4 (1978).
[6] R. J. Gulley and S. J. Buckman, J. Phys. B **27**, 1833 (1994).
[7] M. Zubek, S. Kadifachi, and J. B. Hasted, in *Book of Abstracts of the First European Conference on Atomic and Molecular Physics, Heildelberg, West Germany*, edited by J. Kowalski, G. zu Putlitz, and H. G. Weber (1981), p. 763.
[8] C. Szmytkowski and K. Maciag, Chem. Phys. Lett. **124**, 463 (1986).
[9] C. Szmytkowski, P. Mozejko, and A. Krzysztofowicz, Radiat. Phys. Chem. **68**, 307 (2003).
[10] V. F. Sokolov and Y. A. Sokolova, Pis'ma Zh. Tekh. Fiz. **7**, 627 (1981) [Sov. Tech. Phys. Lett. **7**, 268 (1981)].
[11] L. Sanche and G. J. Schulz, J. Chem. Phys. **58**, 479 (1973).
[12] D. Simon, R. Azria, and M. Tronc, J. Phys. B **11**, L561 (1978).
[13] L. Andric, I. M. Cadez, R. I. Hall, and M. Zubeck, J. Phys. B **16**, 1837 (1983).
[14] M. Gupta and K. L. Baluja, Phys. Rev. A **73**, 042702 (2006).
[15] F. A. Gianturco, P. Paioletti, and N. Sanna, J. Phys. B **30**, 4535 (1997).
[16] A. P. P. Natalense, M. T. do N. Varella, M. H. F. Bettega, L. G. Ferreira, and M. A. P. Lima, J. Phys. B **32**, 5523 (1999).
[17] L. E. Machado, R. T. Sugohara, A. S. dos Santos, M.-T. Lee, I. Iga, G. L. C. de Souza, M. G. P. Homem, S. E. Michelin, and L. M. Brescansin, Phys. Rev. A **84**, 032709 (2011).
[18] A. Zecca, J. C. Nogueira, G. P. Karwasz, and R. S. Brusa, J. Phys. B **28**, 477 (1995).
[19] D. Shi, J. Sun, Y. Liu, Z. Zhu, and X. Yang, Chin. Opt. Lett. **4**, 192 (2006).
[20] D. Raj and S. Tomar, J. Phys. B **30**, 1989 (1997).
[21] C. G. Limbachiya, M. Vinodkumar, and N. J. Mason, Phys. Rev. A **83**, 042708 (2011).
[22] M. Vinodkumar, H. Bhutadia, B. Antony, and N. Mason, Phys. Rev. A **84**, 052701 (2011).
[23] J. Tennyson, At. Data Nucl. Data Tables **64**, 253 (1996).
[24] A. Jain, Phys. Rev. A **34**, 3707 (1986).

[25] A. Jain and K. L. Baluja, Phys. Rev. A **45**, 202 (1992).
[26] M. Vinodkumar, C. G. Limbachiya, K. N. Joshipura, and N. Mason, Eur. Phys. J. D **61**, 579 (2011).
[27] [http://www.nist.gov/chemistry-portal.cfm].
[28] J. Tennyson, Phys. Rep. **491**, 29 (2010).
[29] W. M. Flicker, O. A. Mosher, and A. Kuppermann, J. Chem. Phys. **69**, 3910 (1978).
[30] L. Vuśković and S. Trajmar, J. Chem. Phys. **77**, 5436 (1982).
[31] J. Tennyson, D. B. Brown, J. M. Munro, I. Rozum, H. N. Varambhia, and N. Vinci, J. Phys.: Conf. Ser. **86**, 012001 (2007).
[32] A. M. Arthurs and A. Dalgarno, Proc. Phys. Soc. London A **256**, 540 (1960).
[33] A. Faure, J. D. Gorfinkiel, L. A. Morgan, and J. Tennyson, Comput. Phys. Commun. **144**, 224 (2002).
[34] M. Gailitis, J. Phys. B **9**, 843 (1976).
[35] M. Vinodkumar, R. Dave, H. Bhutadia, and B. Antony, Int. J. Mass Spectrom. **292**, 7 (2010).
[36] M. Vinodkumar, K. N. Joshipura, C. G. Limbachiya, and B. K. Antony, in *Atomic Structure and Collision Processes*, edited by M. Mohan (Narosa Publishing House, New Delhi, 2009), pp. 177–188.
[37] H. L. Cox Jr., and R. A. Bonham, J. Chem. Phys. **47**, 8 (1967).
[38] S. Hara, J. Phys. Soc. Jpn. **22**, 710 (1967).
[39] X. Zhang, J. Sun, and Y. Liu, J. Phys. B **25**, 1893 (1992).
[40] G. Staszewska, D. M. Schwenke, and D. G. Truhlar, J. Chem. Phys. **81**, 3078 (1984).
[41] G. Garcia and F. Blanco, Phys. Rev. A **62**, 044702 (2000).
[42] G. Garcia and F. Manero, Chem. Phys. Lett. A **280**, 419 (1997).
[43] M. Vinodkumar, K. Korot, and P. C. Vinodkumar, Int. J. Mass Spectrom. **305**, 26 (2011).
[44] C. J. Joachain, *Quantum Collision Theory* (North-Holland, Amsterdam, 1983).
[45] M. S. Dababneh, Y.-H. Hsieh, W. E. Kauppila, C. K. Kwan, and T. S. Stein, in *Third International Workshop on Positron (Electron)-Gas Scattering* (World Scientific, Detroit, MI, 1985), p. 251.
[46] J. K. Olthoff, R. H. van Brunt, X. H. Wan, and J. H. Moore, in *Proceedings of the Joint Symposium in Electron and Ions Swarms and Low Energy Electron Scattering*, Gold Coast, Australia, 1991, pp. 25–27.